Importance of momentum dependent interactions in multifragmentation

Suneel Kumar and Rajeev K. Puri
Physics Department, Panjab University, Chandigarh-160 014, India
(Received 4 February 1999; published 1 October 1999)

We analyze the role of different equations of state and momentum dependent interactions in fragmentation. Heavy ion collisions are simulated using a quantum molecular dynamics model and fragments are constructed with the minimum spanning tree method. A detailed study is carried out for Xe+Sn reactions at incident energies $E=100$ and 400 MeV/nucleon and over a wide range of impact parameters. Our analysis indicates that the light mass fragments in central collisions are sensitive towards different static equations of state whereas the heavy fragments are insensitive towards different static equations of state. The results with momentum dependent interactions are quite different. Now, the heavy fragments are also sensitive towards different equations of state. The momentum dependence of the equation of state is able to break the spectator matter into a large number of fragments at peripheral collisions whereas a simple static equation of state fails to produce any fragments. As a result, the properties of fragments (such as transverse flow, rapidity distribution, etc.) are also affected by the momentum dependence of the interaction. [S0556-2813(99)05110-9]

PACS number(s): 25.70.Pq, 24.10.Lx

I. INTRODUCTION

Knowledge of the compressibility of nuclear matter [or in general about the nuclear equation of state (EOS)] is not only relevant for nuclear physics but is also of importance for the understanding of many astrophysical problems such as the stability of neutron stars, the dynamics of supernova explosions, etc. Several experimental and theoretical attempts were made in the past in heavy ion physics to pin down the form of the EOS [1–7]. Unfortunately, most of the observables of heavy ion reactions are insensitive towards different forms of the equation of state and, hence, the final answer to the question of the equation of state is still far from settled [1]. Apart from different equations of state, the momentum dependence of the equation of state has also attracted a lot of consideration [1,4,5,7]. The momentum dependent interactions are found to affect the collective flow quite drastically [1,4]. As a result of the sizable reduction in the baryon-baryon collisions with momentum dependent interactions, subthreshold particle production is also strongly reduced [1,4,7,8]. Furthermore, other observables (such as the rapidity distribution, anisotropy ratio, etc.) are also affected by the momentum dependence of the equation of state. Note that most of the above-mentioned observables are insensitive towards different forms of the equation of state.

During the initial phase of the collision (when two nuclei with large relative momentum penetrate each other), the effect of the momentum dependent interactions is very strong. The particles propagating with momentum dependent interactions are accelerated in the transverse direction during the early phase of the reaction. As a result, fewer collisions take place and the transverse flow increases considerably.

Although a lot of work has been done to understand the role of momentum dependent interactions in observables such as collective flow and particle production, little attention has been paid to understand their role in multifragmentation which is a very fast emerging field of heavy ion physics at intermediate energies [5,7]. In most of the studies on multifragmentation, one has confined oneself to simple static equations of state [1,6,7,9–11]. There are couple of calculations reported in the literature where momentum dependent interactions are used to investigate fragmentation [5,7]. Unfortunately, these studies are confined to central collisions only. Apart from this, the calculations with momentum dependent interactions are coupled with a reduced cross section [5] and hence a definite conclusion about the role of momentum dependent interactions in multifragmentation cannot be drawn. It is very important to analyze the formation of the fragments by employing a variety of equations of state and momentum dependence. The success of the simulations allows us to take the following strategy in extracting the nuclear equation of state: One starts with a simple form of the nuclear equation of state which has a couple of parameters that are specified by the global properties of nuclear matter (i.e., by fitting the binding energy, saturation densities, etc.). The different compressibilities lead to different equations of state. By simulating the heavy ion collisions with different EOS's one can study the effect of different equations of state and of the momentum dependent interactions. In this paper, we follow the same style; i.e., we fix the nucleon-nucleon cross section and simulate the heavy ion collision with variety of equations of state and study the formation of the fragments. This will give us a possibility to check the role of different equations of state and momentum dependent interactions in multifragmentation. The heavy ion collisions are simulated using the quantum molecular dynamics model and the fragments are constructed with the space correlation method.

In the following, we first discuss the quantum molecular dynamics (QMD) model and the momentum dependence of the interaction and then present our results.

II. QMD AND THE MOMENTUM DEPENDENT INTERACTIONS

The quantum molecular dynamics model simulates the reaction on an event by event basis [1]. This is based on the molecular dynamics picture where nucleons interact via two-

TABLE I. Parameters of static and momentum dependent potentials.

K (MeV)	α (MeV)	β (MeV)	γ	δ (MeV)	ϵ	EOS
200	−356	303	1.17	—	—	*S*
380	−124	70.5	2	—	—	*H*
200	−390	320	1.14	1.57	21.54	SMD
380	−130	59	2.09	1.57	21.54	HMD

and three-body interactions. Explicit two- and three-body interactions lead to the preservation of the fluctuations and correlations which are important for *N*-body phenomena such as multifragmentation [1,5,9–11].

In QMD, the (successfully) initialized nuclei are boosted towards each other with proper center-of-mass velocity using relativistic kinematics. Here each nucleon α is represented by a Gaussian wave packet with a width $\sqrt{L}$ centered around the mean position $\vec{r}_\alpha(t)$ and mean momentum $\vec{p}_\alpha(t)$ [1]:

$$\phi_\alpha(\vec{r},\vec{p},t)=\frac{1}{(2\pi L)^{3/4}}e^{\{-[\vec{r}-\vec{r}_\alpha(t)]^2/4L\}}e^{[i\vec{p}_\alpha(t)\cdot\vec{r}/\hbar]}. \quad (1)$$

The Wigner distribution of a system with A_T+A_P nucleons is given by

$$f(\vec{r},\vec{p},t)=\sum_{\alpha=1}^{A_T+A_P}\frac{1}{(\pi\hbar)^3}e^{\{-[\vec{r}-\vec{r}_\alpha(t)]^2/2L\}}e^{\{-[\vec{p}-\vec{p}_\alpha(t)]^2 2L/\hbar^2\}'}, \quad (2)$$

with $L=1.08$ fm^2. The different values of L do not affect the nuclear dynamics.

The center of each Gaussian (in coordinate and momentum space) is chosen by the Monte Carlo procedure. The momentum of nucleons (in each nucleus) is chosen between zero and the local Fermi momentum $[=\sqrt{2m_\alpha V_\alpha(\vec{r})};\ V_\alpha(\vec{r})$ is the potential energy of nucleon $\alpha]$. Naturally, one has to take care that the nuclei thus generated have the right binding energy and proper root mean square radii.

The centriod of each wave packet is propagated using the classical equation of motion [1]:

$$\frac{d\vec{r}_\alpha}{dt}=\frac{dH}{d\vec{p}_\alpha}, \quad (3)$$

$$\frac{d\vec{p}_\alpha}{dt}=-\frac{dH}{d\vec{r}_\alpha}, \quad (4)$$

where the Hamiltonian is given by

$$H=\sum_\alpha\frac{\vec{p}_\alpha^{\,2}}{2m_\alpha}+V^{\rm tot}. \quad (5)$$

Our total interaction potential $V^{\rm tot}$ reads as

$$V^{\rm tot}=V^{\rm loc}+V^{\rm Yuk}+V^{\rm Coul}+V^{\rm MDI}, \quad (6)$$

with

$$V^{\rm loc}=t_1\delta(\vec{r}_1-\vec{r}_2)+t_2\delta(\vec{r}_1-\vec{r}_2)\,\delta(\vec{r}_1-\vec{r}_3), \quad (7)$$

$$V^{\rm Yuk}=t_3e^{-|\vec{r}_1-\vec{r}_2|/m}/(|\vec{r}_1-\vec{r}_2|/m), \quad (8)$$

with $m=1.5$ fm and $t_3=-6.66$ MeV.

In nuclear matter, the static (local) Skyrme interaction reduces to

$$U^{\rm loc}=\alpha\left(\frac{\rho}{\rho_0}\right)+\beta\left(\frac{\rho}{\rho_0}\right)^2. \quad (9)$$

The above two parameters (α,β) are fixed by the requirement that the average binding energy (at normal nuclear matter density ρ_0) should be -15.76 MeV and the total energy should have a minimum at ρ_0. In order to understand the role of different compressibilities, the above potential can be generalized to

$$U^{\rm loc}=\alpha\left(\frac{\rho}{\rho_0}\right)+\beta\left(\frac{\rho}{\rho_0}\right)^\gamma. \quad (10)$$

The momentum dependent interaction is obtained by parametrizing the momentum dependence of the real part of the optical potential. The final form of the potential reads as [1,4]

$$U^{\rm MDI}\approx t_4\ln^2[t_5(\vec{p}_1-\vec{p}_2)^2+1]\,\delta(\vec{r}_1-\vec{r}_2). \quad (11)$$

Here $t_4=1.57$ MeV and $t_5=5\times10^{-4}$ MeV^{-2}. A parametrized form of the local plus momentum dependent interaction (MDI) potential (at zero temperature) is given by

$$U=\alpha\left(\frac{\rho}{\rho_0}\right)+\beta\left(\frac{\rho}{\rho_0}\right)^\gamma+\delta\ln^2[\epsilon(\rho/\rho_0)^{2/3}+1]\rho/\rho_0. \quad (12)$$

The different parameters appearing in Eq. (12) are summarized in Table I. The (additional) momentum dependence of the interaction generates extra repulsion during the evolution of the reaction which increases the collective flow and supresses the subthreshold particle production. This effect is the largest during the initial phase of the reaction.

The imaginary part of the potential is parametrized in terms of nucleon-nucleon cross section. Very recently, a detailed study of the multifragmentation with different *NN* cross sections was carried out by us [10]. This study revealed that different forms of *NN* cross sections have a sizable effect on the multiplicity of the fragments at peripheral collisions. As our present aim is to look at the role of different EOS's and their momentum dependence in fragment production, we use the energy dependent *NN* cross section fitted by Cugnon and implemented by Aichelin [1].

III. RESULTS AND DISCUSSION

The phase space of the nucleons is calculated using Eqs. (3) and (4). Here simulations are performed with different equations of state (i.e., with static soft and hard and the momentum dependent soft and hard, respectively). During the time evolution, two nucleons share the same fragment if their centroids are closer than 4 fm. In a very recent study, we extended the above concept by putting the constraints in momentum space also [9]. In one case, the nucleons with large relative momenta were denied to be a part of the same fragment whereas in other case each fragment was subjected to a binding energy check. In this case, the nucleons of a fragment which fails to pass the binding energy check were treated as free nucleons. The impact of these modifications was drastic in central collision whereas a small effect was seen in peripheral collisions.

The momentum dependent interactions generate additional repulsion which is similar to that generated by the in-medium mean-field-like G matrix [12]. This additional repulsion in the potential is reported to destablize the nuclei and, thus, the nuclei propagating with momentum dependent interactions (in a Vlasov mode) are found to emit nucleons after some hundred fm/c. In order to check the degree of this instability, we carried out a few checks: In the first case, we followed the root mean square radii of Nb, Xe, and Au nuclei propagating with different interactions. We find that all nuclei are reasonably stable until 200 fm/c irrespective of the equation of state used. In some cases, the momentum dependent interactions destablize the nuclei. A further check was made in the form of the binding energy of nuclei. The binding energy of the above-mentioned nuclei was nearly the same for hard and soft equations of state whereas the nuclei propagating with momentum dependent interactions were less stable compared to static interactions. The nuclei propagating with momentum dependent interactions yield a typical binding energy of -5 MeV/nucleon at 200 fm/c compared to -8 MeV/nucleon at the start. This indicates the destabilization of the nuclei propagating with MDI's.

One of the crucial factors governing the formation of the fragment is the nucleons bound in a fragment and their surrounding environment [10,11]. This can be understood by studying the average density which is defined as

$$\langle \rho \rangle = \left\langle \frac{1}{N} \sum_{\alpha=1}^{N} \sum_{\beta=1}^{N} \frac{1}{(2\pi L)^{3/2}} e^{-(\vec{x}_\alpha - \vec{x}_\beta)^2/2L} \right\rangle, \qquad (13)$$

with x_α being the position coordinate of nucleon α. Note that in our above definition [Eq. (13)], every free nucleon has a ''self-density'' of $1/(2\pi L)^{3/2} = 0.32\rho_0$. In Fig. 1, we display the average density $\langle \rho/\rho_0 \rangle$ calculated for Xe+Sn collisions at 100 and 400 MeV/nucleon, respectively. We display the results using static soft and hard (S,H) and soft and hard with MDI's (SMD and HMD), respectively. The upper and lower parts of Fig. 1 are at $b=0$ and 8 fm, respectively. The $b=0$ is a central collision whereas $b=8$ fm indicates the geometry at peripheral collision. One finds that the saturation density in the central collision is nearly independent of the form of EOS. A strong dependence of the equation of state

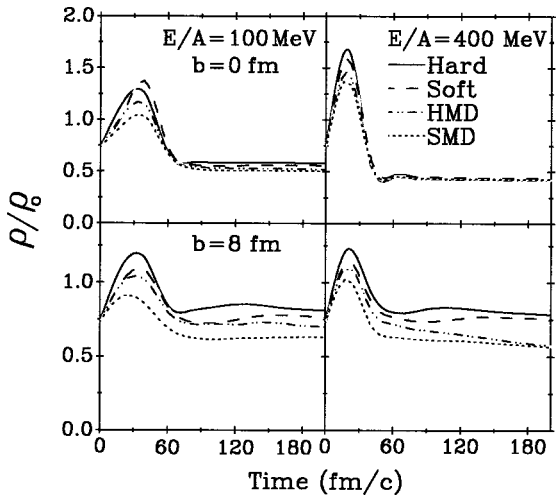

FIG. 1. The average mean density (ρ/ρ_0) as a function of time. The left and right parts of the figure are at 100 and 400 MeV/nucleon, respectively. The upper part displays the result at $b=0$ fm whereas the lower part is at $b=8$ fm. The static hard (H), soft (S), and hard and soft with momentum dependent interactions (HMD and SMD) are indicated by solid, dashed, dash-double-dotted, and dotted lines, respectively.

on density can be seen at peripheral collisions. As a result of repulsive MDI's, the density in the overlap region will be lower compared to the static one. In the central collision at (relative) higher incident energies (i.e., 400 MeV/nucleon), the nucleon-nucleon collisions are more frequent which results in complete destruction of the initial correlations. Therefore, an additional repulsion (due to MDI's) does not alter the results. The effect is drastic at peripheral collisions. Here we see that the difference in the saturation density is about 30%. The initial correlations among nucleons (of each nucleus) are preserved in static interactions which keeps the matter together and thus the density is higher. As soon as the momentum dependence of the interaction is taken into account, the nuclear matter shatters due to repulsion which leads to a lower saturation density and fewer nucleon-nucleon collisions. One also notices that the different equations of state (i.e., the hard and the soft equations of state) have a lesser effect compared to the one with and without momentum dependence of the interaction. In other words, different equations of state result in nearly the same saturation density, but the same EOS with and without MDI's results in a different saturation density.

The collision history for the simulations of Xe+Sn at 400 and 100 MeV/nucleon is displayed in Fig. 2. Here we show the results with S and SMD, respectively. We see that in both cases, the maximum collisions occur between 40 and 50 fm/c. A small shift in the time scale at 100 MeV/nucleon compared to 400 MeV/nucleon is due to the low nucleon velocity at 100 MeV/nucleon. The striking result is that the number of NN collisions at 100 MeV/nucleon is finite even after 150 fm/c whereas no collision occurs after 60 fm/c at 400 MeV/nucleon. Naturally, the maximal collision rate is much higher at 400 MeV/nucleon compared to the one at 100 MeV/nucleon. At 100 MeV/nucleon, the MDI does not produce different collision rate whereas quite different re-

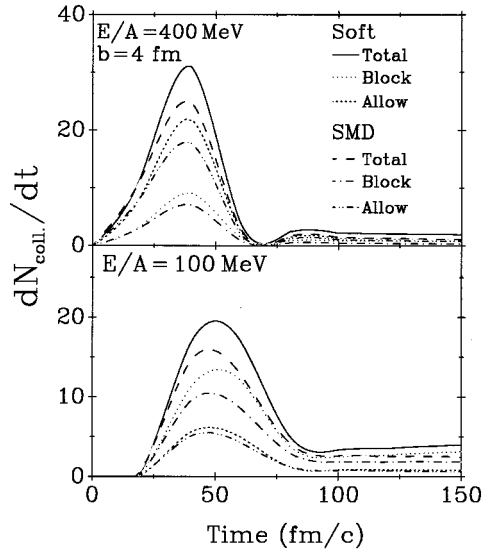

FIG. 2. The rate of collisions ($dN_{\rm coll}/dt$) as a function of time. The collision rate with and without Pauli blocking is also shown.

sults can be seen at 400 MeV/nucleon.

The formation of the fragments and their multiplicities are discussed in Fig. 3. Here we use *S*, *H*, SMD, and HMD, respectively. The displayed results are at 100 MeV/nucleon. We here display the heaviest fragment $A^{\rm max}$, the emitted nucleons, the light mass fragments (LMF's) ($2 \leqslant A \leqslant 4$), the medium light fragments (MLF's) ($5 \leqslant A \leqslant 9$), the medium heavy fragments (MHF's) ($10 \leqslant A \leqslant 19$), the fragment with mass $5 \leqslant A \leqslant 20$, the heavy mass fragments (HMF's) ($21 \leqslant A \leqslant 65$), and the intermediate mass fragments (IMF's) ($5 \leqslant A \leqslant 65$). All displayed multiplicities are at 200 fm/c. We see a well-established behavior of $A^{\rm max}$. It increases with an increase in the impact parameter whereas the emission of nucleons decreases with an increase in the impact parameter. As a result, the LMF's, MLF's, and MHF's also decrease with an increase in the impact parameter. The $A^{\rm max}$ is heaviest using a soft EOS which is followed by the hard EOS and their momentum dependent interactions. As a result of an additional repulsion, a lot of nucleons are emitted in the HMD which is followed by SMD/hard/soft EOS. The most interesting results are concerning the HMF and IMF production. In both cases, we see that the SMD has a clear edge over other interactions. The apparent cause seems to be that in central collisions, a large destruction of the initial correlations already takes place and hence additional momentum dependence further destroys the remaining correlations which reduces the multiplicity of the IMF's and HMF's. Note that this leads to the emission of a lot of nucleons and LMF's. On the contrary, the momentum dependent interactions break the heavy fragments into a large number of intermediate mass fragments in peripheral collisions, leading to a lot of IMF's and HMF's.

Figure 4 displays the same results as the ones reported in Fig. 3, but at 400 MeV/nucleon. Here $A^{\rm max}$, free nucleons, and LMF's behave in the same way as reported at 100 MeV/nucleon. We also see a well-known rise and fall in the multiplicity of fragments with a change in the impact parameter.

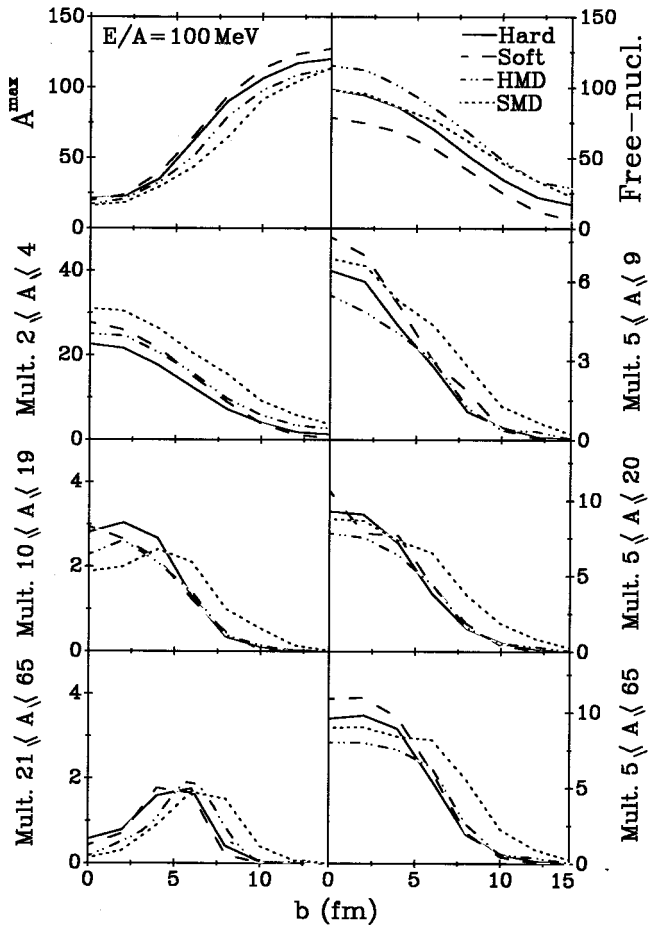

FIG. 3. The $A^{\rm max}$, multiplicity of free nucleons, LMF's ($2 \leqslant A \leqslant 4$), MLF's ($5 \leqslant A \leqslant 9$), MHF's ($10 \leqslant A \leqslant 19$), $5 \leqslant A \leqslant 20$, HMF's ($21 \leqslant A \leqslant 65$), and IMF's ($5 \leqslant A \leqslant 65$) as a function of impact parameter b. The displayed quantities are at 200 fm/c. Here simulations with soft (dashed line), hard (solid lines), SMD (dotted line), and HMD (dashed-double dotted line) are at 100 MeV/nucleon.

A similar behavior can also be seen in case of MHF's and HMF's. We see that the momentum dependent interactions yield fewer fragments in central collisions, whereas a lot of IMF's are produced in the simulation at peripheral collisions. In peripheral collisions, the static hard and soft EOS's are not able to break the initial correlations among nucleons and hence no IMF's are emitted. As soon as the momentum dependence of the interaction is taken into account, the initial correlations among nucleons are destroyed which results in a large number of IMF's. From Figs. 3 and 4, it is also clear that the only quantity which is sensitive to different equations of state is the light mass fragments in central collisions. One sees that LMF's production in central collisions is quite different with hard and soft equations of state. This difference washes away when one goes to peripheral collisions or to heavy mass production. In view of this, light mass fragment production (in central collisions) can be very useful to pin down the equation of state through multifragmentation.

The difference in the multiplicity of the heavy mass fragments using *S* and *H* is larger if the momentum dependence of the interaction is taken into account. This difference is

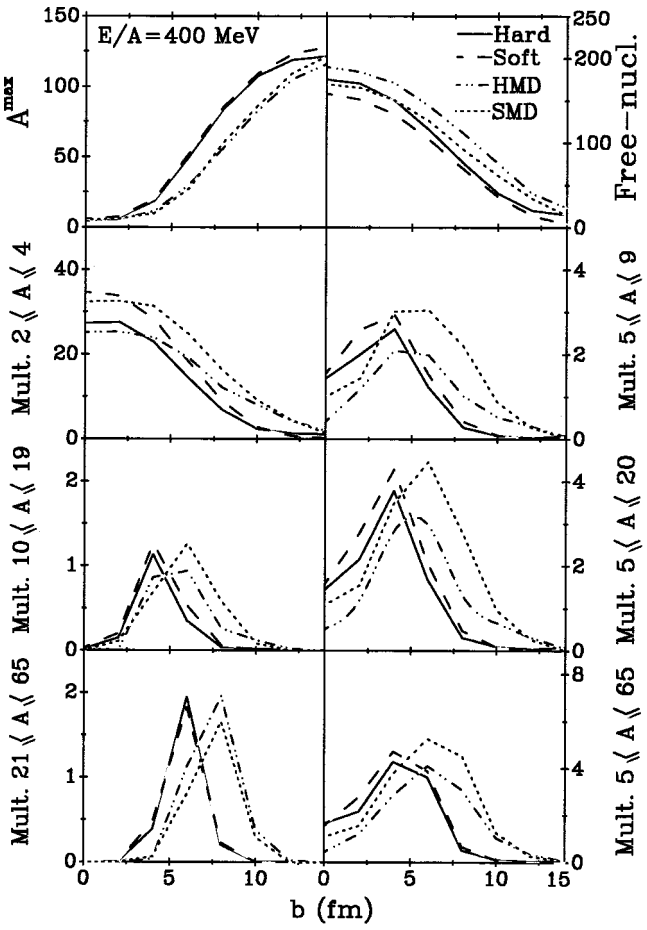

FIG. 4. Same as Fig. 3, but at 400 MeV/nucleon.

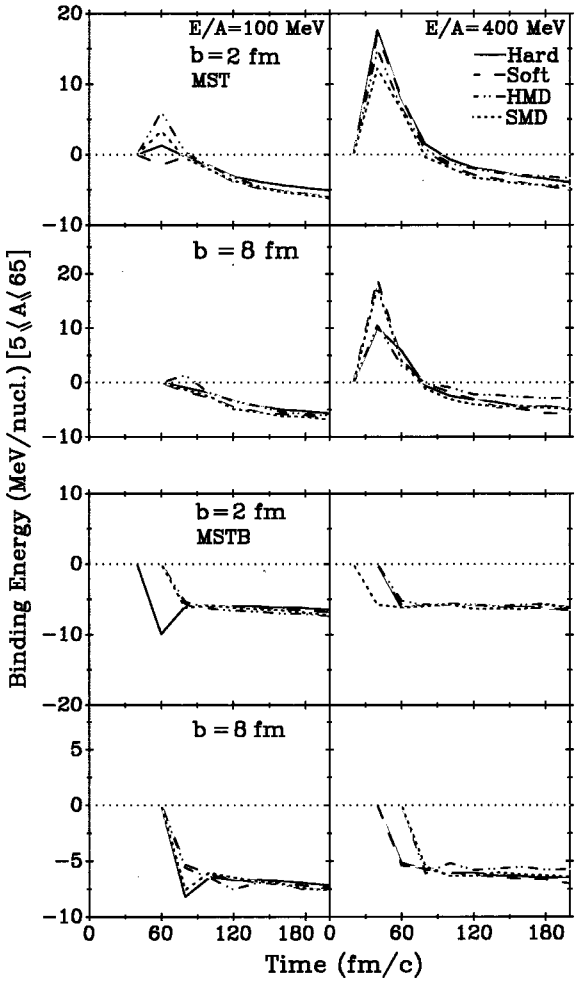

FIG. 5. The binding energy per nucleon (calculated in the center of mass of a fragment) as a function of time. The left and right parts are at 100 and 400 MeV/nucleon, respectively. The upper and lower parts are with normal MST and MSTB, respectively.

encouraging as it can give a clue about the equation of state. One also sees that IMF production at peripheral collisions is very sensitive to MDI's. These results clearly indicate that the simple soft/hard interactions do not break the spectator matter into IMF's. Note that the simple static hard and soft equations of state fail to transfer the energy from the participant region to the spectator region. This means that one will observe very few heavy fragments and a couple of light fragments with static interaction. When MDI's are taken into account, the heavy fragments break into intermediate mass fragments. A similar result can also be obtained if one takes into account a larger *NN* cross section [10]. With a larger value of the *NN* cross section, additional transfer of the momentum occurs. Note that in the case of the disappearance of the flow (the attractive interactions at low energy balance the repulsive interactions at higher energies, and thus the flow disappears [13,14]), one needs a momentum dependent interaction to explain the experimentally observed balance energies at peripheral collisions [14]. All these studies indicate the importance of the momentum dependent interactions in heavy ion collisions at peripheral collisions. It is also interesting to note that the difference in the results using soft and hard equations of state increases when MDI's are taken into account. Therefore, different equations of state can be extracted more accurately if MDI's are present. The enhancement in the production of intermediate mass fragments is encouraging because in a recent ALADIN experiment [2], a simple soft/hard EOS is reported to underestimate the IMF production at larger impact parameters. Therefore, MDI's can help to resolve this puzzle.

It would be of further interest to check the stability of the fragments produced in the simulations of heavy ion collisions. The time evolution of the average binding energy of the fragments (calculated in their respective center of masses) is displayed in Fig. 5. The left and the right parts of the figure display the results at 100 and 400 MeV/nucleon, respectively. The upper part of the figure shows the binding energy of the fragments detected with the MST algorithm whereas the lower part of the figure displays the binding energy of fragments calculated with the extended MST algorithm where the fragments identified with the normal MST are further subjected to a binding energy check. The nucleons of any fragment which fails to pass the binding energy check are treated as free nucleons. This method was dubbed minimum spanning tree binding (MSTB) [9]. The interesting

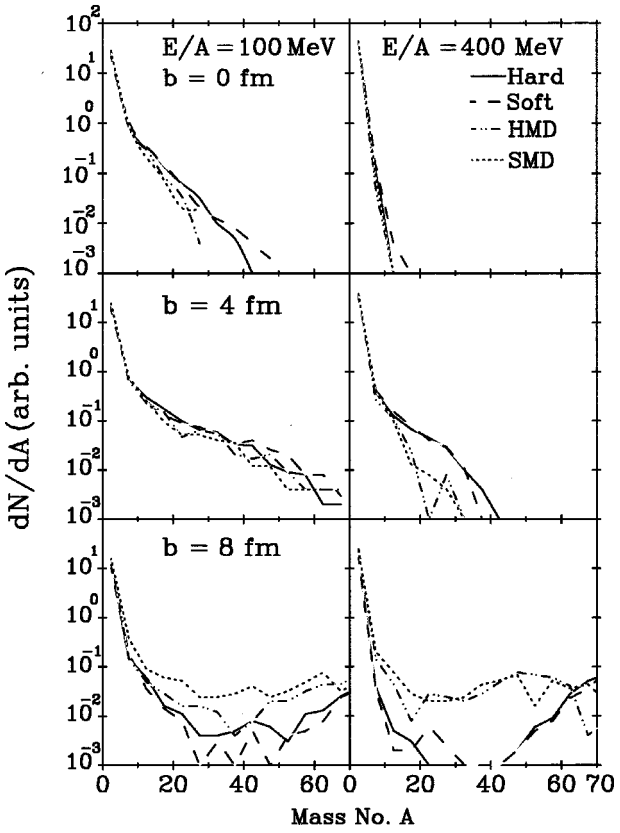

FIG. 6. The mass distribution of the fragments. Here we display the results at 100 MeV/nucleon (left part) and 400 MeV/nucleon (right part), using a different form of the equations of state and MDI's included in it.

point is that the binding energy of the fragments calculated with different EOS's is nearly the same. In some cases, the fragments produced in the simulation with MDI's are more stable. It is worth mentioning that the IMF's are more bound compared to the LMF's. This is quite understandable as the IMF's are the remanant of the spectator matter whereas LMF's are produced in a collision. From the above discussion, it is clear that the stability of the fragments is not affected by the nature of the interaction used.

Figure 6 shows the mass distribution of the fragments at three different impact parameters. The left and right parts of the figure are at 100 and 400 MeV/nucleon, respectively. We see that the static interactions produce far more intermediate mass fragments in central collisions ($b=0-4$ fm) whereas the momentum dependent interactions produce more fragments in peripheral collisions. It was also evident from Figs. 3 and 4 where the multiplicity of various fragments was displayed. These results depict the importance of the momentum dependent interactions in peripheral collisions. One also sees an increase in the slope with an increase in the impact parameter and energy.

Finally, we discuss the properties of the fragments produced in the simulation of heavy ion collisions with different equations of state and momentum dependent interactions. Figure 7 displays the rapidity distribution of the fragments at 400 MeV/nucleon. We define the rapidity distribution as

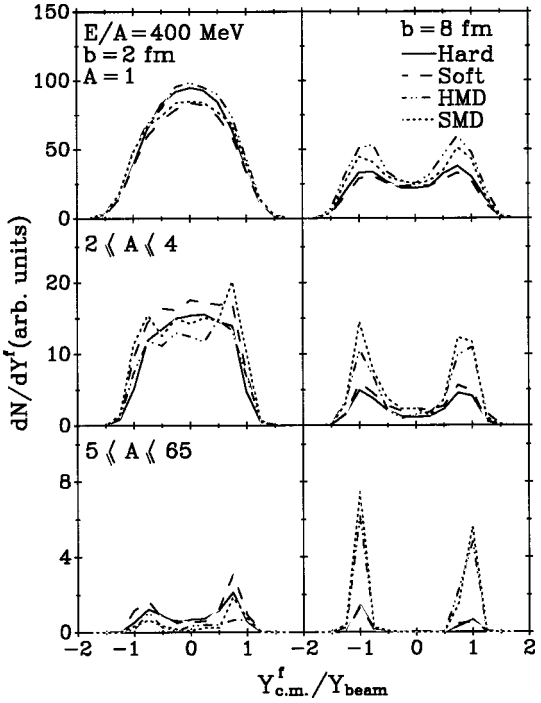

FIG. 7. The rapidity distribution of fragment dN/dY^f as a function of $Y^f_{\rm c.m.}/Y_{\rm beam}$. The displayed results are at 400 MeV/nucleon.

$$Y_j^f=\frac{1}{2}\ln\frac{E^f(j)+p_z^f(j)c}{E^f(j)-p_z^f(j)c}. \tag{14}$$

Here E^f and p_z^f are the mean energy and the longitudinal momentum of the fragments. The rapidity of the free nucleons is largest with momentum dependent interactions. Naturally, a soft EOS produces less repulsion and, hence, fewer nucleons. The most striking point is that the rapidity distributions are less affected in central collisions whereas it leads to an entirely different result in peripheral collisions. Naturally at $b=8$ fm, the simple static soft/hard EOS's do not produce IMF's; therefore, we see very small peaks in the rapidity distribution. On the other hand, larger peaks (at target and projectile rapidities) can be seen in the simulations with momentum dependent interactions. These peaks at target and projectile rapidities indicate a nonequilibrium situation.

Figure 8 which displays the directed transverse momentum (averaged over all nucleons/fragments) shows a sizable difference in the directed transverse momentum $\langle p_x^{\rm dir}\rangle$ using soft and hard equations of state. This difference reduces at peripheral collisions. An additional momentum dependence leads to an extra acceleration of the nucleons into the transverse direction, generating more transverse momentum. Note that the maximum $\langle p_x^{\rm dir}\rangle$ occurs at $b=4$ fm.

Finally, in Fig. 9, we show the $dN/p_t dp_t$ as a function of p_t. We see that the light mass fragments have less difference in their momentum distribution compared to heavy fragments. In all cases, the momentum dependence of the interaction has a sizable effect. The momentum distribution of the nucleons with a lower value of p_t is largely affected by the

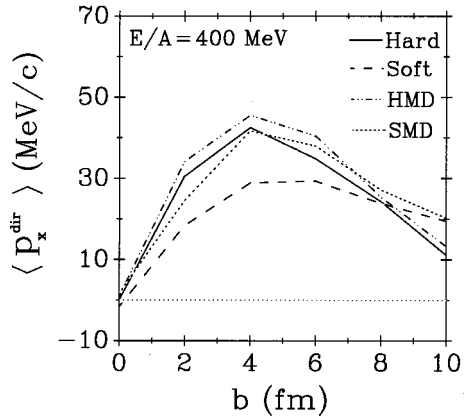

FIG. 8. The directed transverse momentum $\langle p_x^{\mathrm{dir}} \rangle$ as a function of the impact parameter.

momentum dependence of the interaction at peripheral collisions. This effect washes away for a larger value of the p_t.

IV. SUMMARY

Summarizing, we have analyzed the role of different equations of state (namely, hard and soft) and their momentum dependence in multifragmentation. The simulation of the heavy ion collisions is carried out within a quantum molecular dynamics model. The fragments were constructed with a minimum spanning tree description. To study the role of different equations of state and their momentum dependence, we employed static and momentum dependent interactions. We find that the difference in the multiplicity of various fragments using static hard and soft EOS's is only marginal. On the contrary, the difference in the results with and without momentum dependent interactions is quite large. This difference is sizable at peripheral collisions where static interactions fail to produce any IMF's. In addition, the difference in the multiplicity of the fragments with different EOS's is more when their momentum dependence is taken into account. Fragment properties such as the rapidity distribution, directed transverse flow, and transverse momentum distribution are also affected by the momentum dependence of the equation of state.

It is worth mentioning that the nuclei generated with momentum dependent interactions are not as stable as those generated with simple static interactions. Our present (qualitative) study gives, at least, an indication that the fragment production at peripheral collisions is strongly influenced by the momentum dependent interactions. It would, therefore, be of interest to study fragment production with a new algorithm such as the simulated annealing clusterization algorithm [11] which is capable of identifying the fragments as early as 40–60 fm/c and, therefore, the problem of the destablization of the nuclei in MDI's will not rise.

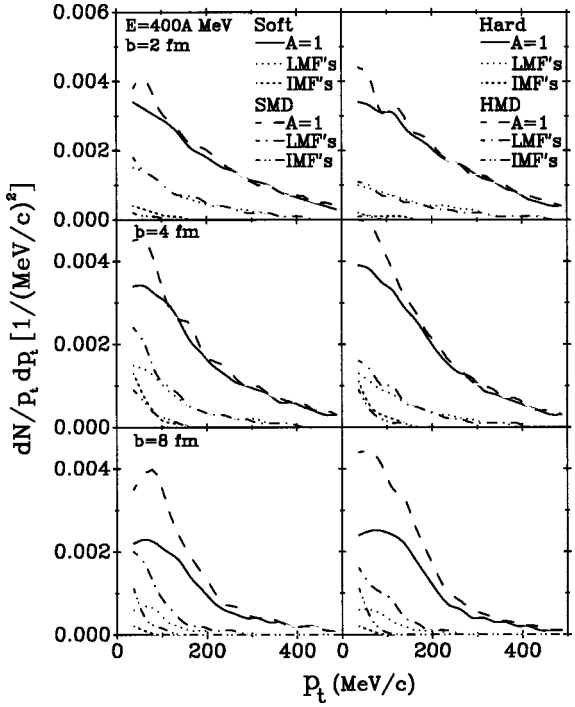

FIG. 9. The $dN/p_t dp_t$ as a function of p_t. Here the left part is with soft (with and without MDI's) and the right part is hard (with and without MDI's).

ACKNOWLEDGMENTS

This work was supported by the Young Scientist Research Grant given to R.K.P.

[1] J. Aichelin, Phys. Rep. **202**, 233 (1991).

[2] C. A. Ogilvie *et al.*, Phys. Rev. Lett. **67**, 1214 (1991); M. B. Tsang *et al.*, *ibid.* **71**, 1502 (1993); R. T. de Souza *et al.*, Phys. Lett. B **268**, 6 (1991); G. F. Peaslee *et al.*, Phys. Rev. C **49**, R2271 (1994); C. Williams *et al.*, *ibid.* **55**, R2132 (1997); A. Schüttauf *et al.*, Nucl. Phys. **A607**, 457 (1996); T. Li *et al.*, Phys. Rev. Lett. **70**, 1924 (1992); K. Hagel *et al.*, *ibid.* **68**, 2141 (1992); N. T. B. Stone *et al.*, *ibid.* **78**, 2084 (1997); B. Jakobsson *et al.*, Nucl. Phys. **A509**, 195 (1990); M. Bagemann-Blaich *et al.*, Phys. Rev. C **48**, 610 (1993); J. Hubble *et al.*, *ibid.* **46**, R1577 (1992); J. Hubble *et al.*, Z. Phys. A **340**, 263 (1991).

[3] B. A. Li and D. H. E. Gross, Nucl. Phys. **A554**, 257 (1993); H. M. Xu, C. A. Gagliardi, R. E. Tribble, and C. Y. Wong, *ibid.* **A569**, 575 (1994); F. Daffin, K. Haglin, and W. Bauer, Phys. Rev. C **54**, 1375 (1996); V. de la Mota, F. Sebille, M. Farine, B. Remaud, and P. Schuck, *ibid.* **46**, 677 (1992); G. F. Bertsch and S. D. Gupta, Phys. Rep. **160**, 189 (1988).

[4] J. Aichelin, A. Rosenhauer, G. Peilert, H. Stöcker, and W. Greiner, Phys. Rev. Lett. **58**, 1926 (1987).

[5] G. Peilert, H. Stöcker, W. Greiner, A. Rosenhauer, A. Bohnet, and J. Aichelin, Phys. Rev. C **39**, 1402 (1989).

[6] T. Maruyama, K. Niita, T. Maruyama, and A. Iwamoto, Prog. Theor. Phys. **98**, 87 (1997).

[7] Ch. Hartnack, Ph.D. thesis, University of Frankfurt, Frankfurt, Germany, 1989.
[8] S. W. Huang, A. Faessler, G. Q. Li, R. K. Puri, E. Lehmann, D. T. Khoa, and M. A. Matin, Phys. Lett. B **298**, 41 (1993); Ch. Hartnack, J. Jaenicke, L. Sehn, H. Stoecker, and J. Aichelin, Nucl. Phys. **A580**, 643 (1994).
[9] S. Kumar and R. K. Puri, Phys. Rev. C **58**, 320 (1998); **58**, 2858 (1998).
[10] S. Kumar, R. K. Puri, and J. Aichelin, Phys. Rev. C **58**, 1618 (1998).
[11] P. B. Gossiaux, R. K. Puri, Ch. Hartnack, and J. Aichelin, Nucl. Phys. **A619**, 379 (1997).
[12] D. T. Khoa, N. Ohtsuka, M. A. Matin, A. Faessler, S. W. Huang, E. Lehmann, and R. K. Puri, Nucl. Phys. **A548**, 102 (1992).
[13] R. Pak *et al.*, Phys. Rev. C **53**, R1469 (1996); S. Kumar, M. K. Sharma, R. K. Puri, K. P. Singh, and I. M. Govil, *ibid.* **58**, 3494 (1998).
[14] S. Soff, S. A. Bass, Ch. Hartnack, H. Stoecker, and W. Greiner, Phys. Rev. C **51**, 3320 (1995).